Xu, Y.; Huang, Y.; Zhong, Z.; You, S.; Gan, W.; Xiao, B.; Maawad, E.; Schell, N.; Gensch, F.; Pan, F.; Hort, N.:

In situ compressive investigations on the effects of solid solution Gd on the texture and lattice strain evolution of Mg.

In: Materials Science and Engineering A. Vol. 774 (2020) 138938.

First published online by Elsevier: 10.01.2020

https://dx.doi.org/10.1016/j.msea.2020.138938

In situ compressive investigations on the effects of solid solution Gd on the texture and lattice strain evolution of Mg

Yuling Xu[1,2,*], Yuanding Huang[2,*], Zhengye Zhong[2], Sihang You[2], Weimin Gan[2], Biquan Xiao[3], Emad Maawad[2], Norbert Schell[2], Felix Gensch[4], Fusheng Pan[1,3], Norbert Hort[2]

[1]Chongqing Academy of Science and Technology, Chongqing 401123, China

[2] Institute of Materials Research, Helmholtz-Zentrum Geesthacht, Max-Planck-Str. 1, 21502 Geesthacht, Germany

[3]Chongqing University, Chongqing 400045, China

[4]TU Berlin, Forschungszentrum Strangpressen, Gustav-Meyer-Allee 25, 13355 Berlin, Germany

Abstract

The present work studies the effects of solid solution Gd on the texture and lattice strain evolution of an extruded Mg15Gd alloy under uniaxial compression. *In situ* experiments were carried out using high energy X-ray diffraction on samples of the investigated materials with three different orientations. The original textures of the pure Mg and the Mg15Gd alloy exhibit basal planes that are preferentially parallel and perpendicular to the extrusion direction (ED), respectively. The c/a ratio of the Mg15Gd alloy decreases with increasing Gd content in the solid solution, leading to a different deformation behavior compared with pure Mg under the compressive load. The addition of Gd enhances the slip and twinning modes. However, prismatic slip is activated earlier in the Mg15Gd alloy due to the lower c/a ratio.

Key words:

Magnesium alloy, Texture, Lattice strain, Compression.

1. Introduction

Mg and its alloys show strong anisotropy due to their hexagonal structures, which results in considerably anisotropic elastic and plastic mechanical properties [1, 2]. The majority of previous research focuses on determining the critical resolved shear stress (CRSS) and shows that the CRSS of non-basal slip systems is much higher than that of basal slip and that of $\{10\bar{1}2\}$ twinning [3, 4]. N. Stanford *et al.* evaluated the effect of Y as a solute strengthener on the Mg alloy and confirmed that Mg–0.5%Y and Mg–2.2%Y alloys have the same CRSS for basal slip and $\{10\bar{1}2\}$ twinning. The Mg–2.2%Y alloy showed a larger CRSS for <c+a> slip [5]. S.R. Agnew worked on the Mg–Y–Nd–Zr and WE43 alloys and explained the effects of precipitations on slip and twinning systems. The prismatic plate-shaped precipitates strongly obstructed basal slip, leading to an increment of over 200% in the CRSS of basal slip [6]. They also studied the slip mechanisms in the AZ31B (Mg–3Al–1Zn) alloy [7]. Their results confirmed that the activation of prismatic slip is much harder than for basal slip and twinning. However, the prismatic slip system tends to be activated in hexagonal close-packed (HCP) metals with a lower c/a ratio, such as titanium and zirconium [8, 9].

In wrought Mg alloys, the lack of <c+a> slips and the predominance of twinning modes result in strong textures. The addition of rare earth elements (Res) can weaken the textures after extrusion, as described in previous publications [10-12]. Among the Res, Gd is highly soluble in Mg, with a maximum solubility of 4.53 at.% at the eutectic temperature [13]. The c/a ratio of the Mg–Gd alloy decreases with increasing content of Gd [14]. With low c/a

ratios, Mg–Gd alloys provide a significant improvement in anisotropy, which exerts considerable influence on the activation of slip systems.

High energy X-ray diffraction provides an effective method for measuring microscale strains. Third generation synchrotron radiation enables the acquisition of microstructural information in a short exposure time. The lattice spacing of individual $\{hkil\}$ lattice planes and textural evolution can be obtained from the Debye-Scherrer rings, which are collected by *in situ* lattice strain and pole figure measurements, respectively. The present work investigated the deformation behavior of a pure Mg and an extruded Mg–15 wt.% Gd alloy using *in situ* synchrotron X-ray diffraction. These two materials have a similar grain size but quite different textures, which sheds light on the effect of Gd solid solution on slip and twinning behaviors in magnesium.

2. Experimental and data evaluation

2.1 Materials

Pure Mg (99.9%) and a Mg–15 wt.% Gd alloy (Mg15Gd) were prepared in this study. The details of the casting processes were reported in a previous publication [14]. The solubility of Gd in solid Mg can reach 4.41 at.% at the eutectic temperature (542 °C). Before hot extrusion, pure Mg and the Mg15Gd alloy were heat treated at 530 °C for 6 and 8 hrs (T4 state), respectively, followed by quenching in water. The hot extrusions were performed at Fachgebiet Metallische Werkstoffe (FMW) in TU Berlin, Germany. The T4 treated billets were machined to cylinders with sizes of 93 mm in diameter and 200 mm in length. After that,

the cylinders were homogenized in an electromagnetic induction furnace at 440 °C. Indirect extrusion was carried out to produce round bars with a 12 mm diameter at 450 °C. The extrusion ratio was 1:60, and the extrusion rate (speed of the extruded bar at the die exit) was set to 0.6 m/s.

Three cylindrical compression samples with sizes of 5 mm in diameter and 10 mm in length were machined from the extruded bars along the extrusion direction ED (0ED), 45º to the ED (45ED) and perpendicular to the ED (90ED), respectively. The compressive direction was parallel to the three directions.

2.2 Microstructural characterizations

High-angle annular dark field scanning transmission electron microscope (HAADF-STEM) characterization was performed on the Mg15Gd alloy using a probe-corrected FEI Titan G^2 60-300 ChemiSTEM operated at 300 KV. The specimens for TEM examination were first ground with SiC paper and then polished with 1 μm and 0.3 μm alumina particles. Next, the final thinning of the specimens was performed by using a precision ion polishing system (GATAN 691).

2.3 Texture measurement using synchrotron radiation

The *in situ* texture measurements were carried out at the Helmholtz-Zentrum Geesthacht GEMS outstation (P07) at Petra III (DESY, Hamburg). A high energy X-ray beam with energy of 87 keV and a beam size of 1 × 1 mm^2 was chosen for the measurements. The sample-detector distance was 1 069 mm. The cylindrical sample was fixed in a universal testing machine (UTM) that can reach a maximum load of 20 kN. The *in situ* compression

measurements were performed at room temperature with a loading speed of 0.0166 mm/s until ultimate compressive strength (UCS). Texture measurements were performed at 4 specific strains which correspond to the following characteristic points: initial elastic deformation (P1), after yielding (P2), at quasi-steady state plastic deformation (P3) and after fracture (P4) (Table 1). During each texture measurement, the loading machine was set under position control. The ω rotation for an incomplete pole figure measurement was from -65° to 65° with 5° per step. Debye-Scherrer rings were collected at each ω angle using a Perkin Elmer XRD 1 622 flat panel, which is a kind of fast read-out area detector that has 2 048 × 2 048 pixels that are 200 μm each. One incomplete pole figure measurement took approximately 5 min. The compression rate was 1×10^{-3} s^{-1}, which was recorded by the software coupled with the UTM. The complete pole figures were calculated from the measured incomplete $\{10\bar{1}0\}$, (0002), and $\{10\bar{1}1\}$ pole figures using the software MTEX [15].

2.4 Lattice strain measurement

The lattice strain measurements were performed at PETRA III (DESY, Hamburg), with an X-ray wavelength of 1.429 nm, a beam size of 1 × 1 mm^2 and sample-detector distance of 1039 mm. The ω angle was fixed at 0º for all the diffraction pattern measurements. The cylindrical sample was fixed in the UTM. The *in situ* compression measurements were performed at room temperature with a loading speed of 0.0166 mm/s, and a step width of 0.6 mm in elongation until UCS. The diffracted beams, Debye-Scherrer rings, were recorded continuously by a Perkin Elmer XRD 1 622 flat panel. The misalignment of the area detector

was corrected by LaB_6 standard powder using the software package Fit2D [16], and the tilting angle of the detector was 0.05º.

The diffraction patterns were collected at each measured point. The Debye-Scherrer rings correspond to the different {*hkil*} lattice planes. To obtain the lattice spacing of different {*hkil*} lattice planes oriented parallel and perpendicular to the compressive direction, the 2θ-intensity spectra of two sectors were generated by integration along these two directions using the software Fit2D. Measuring the lattice spacing at a specific stress provides a way to characterize the lattice strains of differently oriented grains. Diffraction occurs when Bragg's law is satisfied, which has the following expression:

$$2d_{hk\cdot l}\sin\theta_{hk\cdot l} = \lambda$$

where $d_{hk\cdot l}$ is the lattice spacing of specially oriented {*hkil*} lattice planes, $\theta_{hk\cdot l}$ is the diffraction angle of {*hkil*} lattice planes, and λ is the wavelength of the radiation.

The lattice strain of specific {*hkil*} planes can be calculated by the lattice spacing change of the diffraction peak via:

$$\varepsilon_{hk\cdot l} = \frac{d_{hk\cdot l} - d_{0,hk\cdot l}}{d_{0,hk\cdot l}}$$

where $d_{0,hk\cdot l}$ is the lattice spacing of the starting material.

3. Results

3.1 TEM observations and compressive curves

The optical microstructures for the investigated materials, obtained both parallel and perpendicular to the extrusion direction, were presented in a previous work [14]. Both pure Mg and Mg15Gd revealed a homogeneous and fine grain microstructure. The microstructures were almost identical on the sections perpendicular and parallel to the extrusion direction. Only a few second phases could be observed. The grain sizes of the extruded pure Mg and Mg15Gd alloy were 54.5 ± 33.8 μm and 30.6 ± 12.7 μm, respectively.

The HAADF-STEM images in Fig. 1(b) and (c) show the atomic structure of the Mg15Gd alloy corresponding to the points in Fig. 1(a), which were observed from the interior of grain and the grain boundary, respectively. The electron beam is parallel to α(Mg)[0001]. The characteristic hexagonal arrangement of Mg atoms is clearly resolved, while Gd dopants are detected as significantly brighter “dots” in some of the atomic columns. The distributions of Gd atoms in the interior of the grain and on the grain boundary tend to be similar. The same observations were performed on several grains. The Gd-rich columns that normally contain 2~3 Gd atoms were observed, indicating that after 8 hrs of solid solution treatment and the subsequent extrusion, the Gd atoms were almost randomly resolved in the Mg matrix.

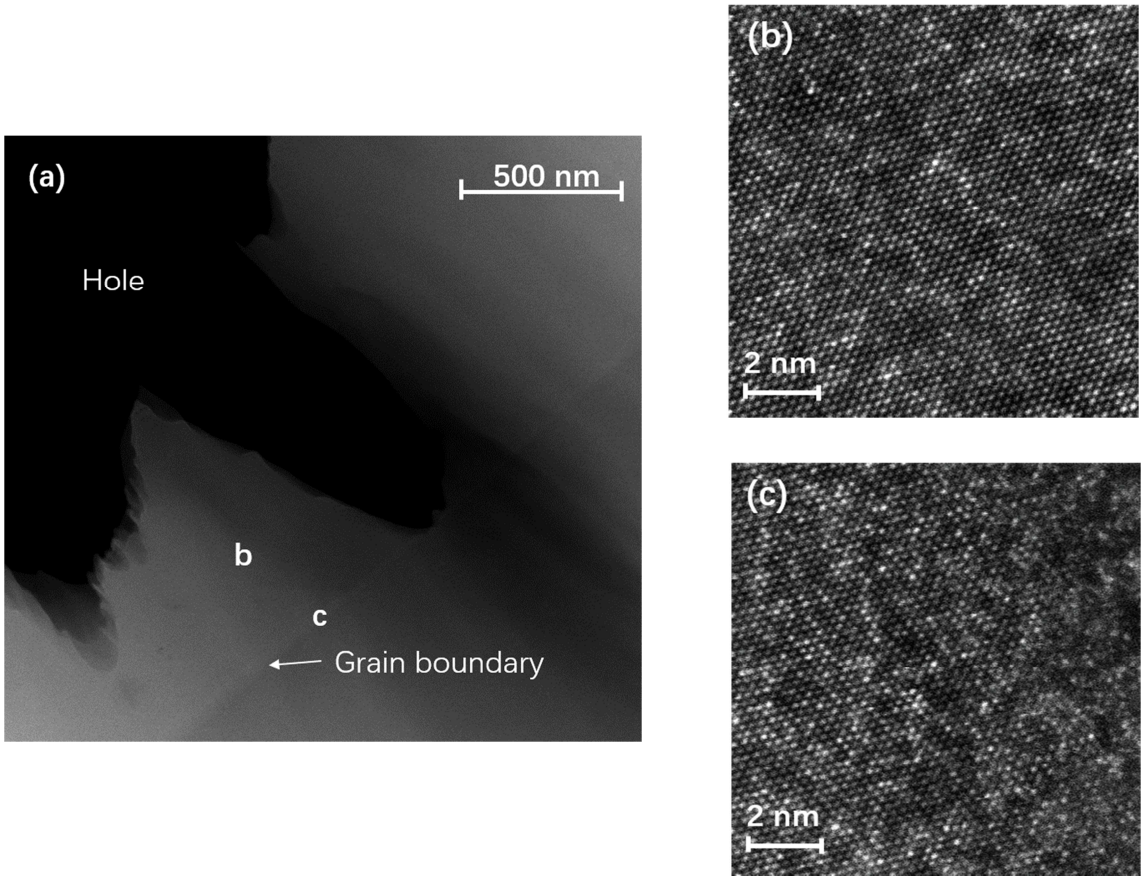

Fig. 1 (a) TEM image of Mg15Gd alloy, and HAADF-STEM images observed (b) in the interior of grain and (c) on the grain boundary. Electron beam is parallel to α(Mg)[0001].

The compressive stress-strain curves of the extruded pure Mg and Mg15Gd alloy with different orientations are shown in Fig. 2. Pure Mg has a low yield strength with a value of approximately 25 MPa for all three orientations. The pure Mg 90ED has a compressibility of 22%, which is 3% higher than that of the 0ED sample. However, the Mg15Gd alloy shows a higher yield strength and different compressibilities for the three orientations. The compressibility of the 90ED sample is approximately 9% higher than that of the ED sample. The Mg15Gd alloy shows elastic behavior up to 225, 175 and 225 MPa for the compressive direction parallel to the ED, 45º to the ED and 90º to the ED of the samples, respectively.

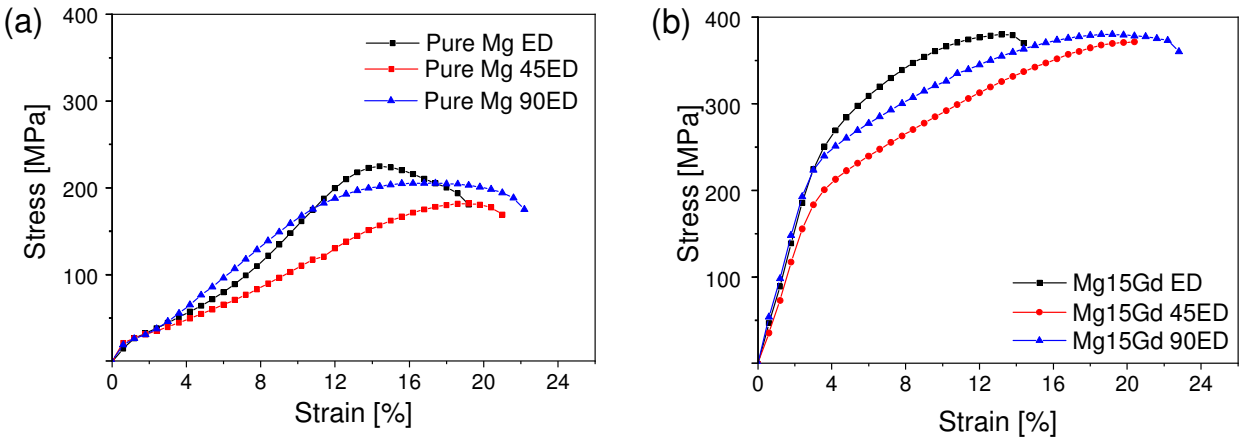

Fig. 2 Engineering stress-strain curves for (a) extruded pure Mg and (b) Mg15Gd alloys.

3.2 Texture evolution

Fig. 3 shows the complete $\{10\bar{1}0\}$, $\{0002\}$ and $\{11\bar{2}0\}$ pole figures of the initial extruded pure Mg and Mg15Gd alloy. The pure Mg exhibited an ED // $<10\bar{1}0>$ fiber texture, which has frequently been observed in many Mg alloys (Fig. 3(a)). The basal planes are distributed in parallel to the extrusion axis [17, 18]. The pole figures clearly show that the basal planes of the Mg15Gd alloy grains were approximately perpendicular to the ED, and these gains laid on the arc between the $\{10\bar{1}0\}$ and $\{11\bar{2}0\}$ planes, parallel to the ED. The Mg15Gd alloy shows a maximum pole figure intensity, i.e., 7.3 multiples of random distribution (mrd), that is much higher than that of pure Mg.

The *in situ* pole figure measurement points during the compressive test, which are represented by P1 to P4 for each sample, are listed in Table 1.

The lattice parameters of each alloy were obtained from *in situ* pole figure measurements for which the ω angle is 0° by using the MAUD software, which is based on the Rietveld method [19]. The results show that the lattice parameters, *a* and *c,* of pure Mg and the Mg15Gd alloy

increase from 0.3209 to 0.3226 and 0.5210 to 0.5218, respectively. However, the *c/a* ratios decrease from 1.6233 to 1.6174 with the addition of Gd. It seems that the isotropy was adjusted by the addition of Gd.

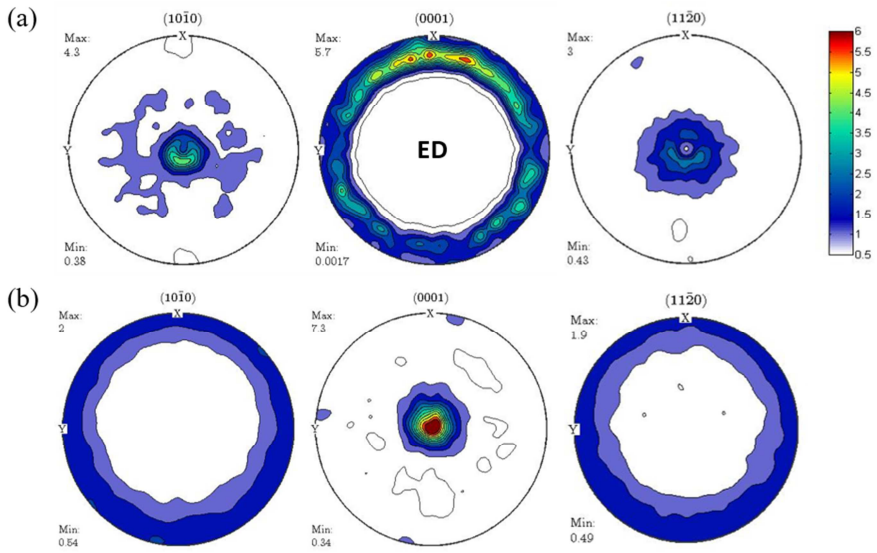

Fig. 3 {10$\bar{1}$0}, {0002} and {11$\bar{2}$0} pole figures of (a) Pure Mg and (b) Mg15Gd alloys.

Table 1 Stress and strain at the texture measurement points.

Point	Pure Mg						Mg15Gd					
	Stress [MPa]			Strain [%]			Stress [MPa]			Strain [%]		
	0ED	45ED	90ED	0ED	45ED	90ED	0ED	45ED	90ED	0ED	45ED	90ED
P1	18.1	18.2	18.0	0.5	0.5	0.4	176.0	176.0	176.0	2.7	3.2	2.8
P2	40.5	38.3	38.6	2.5	2.7	1.2	227.0	227.0	227.0	3.6	5.1	3.7
P3	200.9	73.8	197.7	12.2	6.7	12.2	301.6	303.0	302.3	5.8	11.34	10.6
P4				19.0	20.8	21.4				14.4	20.4	21.0

3.2.1 Compression along the extrusion direction (0ED)

The evolution of the {10$\bar{1}$0} and {0002} pole figures during compression of the ED samples are presented in Fig. 4. The compressive direction is in the pole figure center. Due to the existence of some coarse grains and the limitation of available maximum beam size, few high

pole intensity points are clearly seen in the pole figure. However, the general texture information can be inferred from these pole figures. For pure Mg, from P1 to P2, most of the grains retain their initial orientations, and the pole density of the {0002} pole figure appears at the center (Fig. 3(a)). After increasing the compressive strain to P3, the pole figures show an obvious change under a stress of 200 MPa. The basal planes of most grains were reoriented to be perpendicular to the compressive direction. The maximum pole intensity of the {0002} pole figure increases to 17.0 mrd (multiples of random distribution) in the vicinity of the pole figure center. After fracture (P4), the maximum pole intensity shows a slight increase compared with that for P3.

The basal planes show a distribution that is mostly perpendicular to the load direction in the Mg15Gd alloys (Fig. 4(b)), and a high basal pole intensity of 9 mrd exists at P1 of the initial state; some grains, which are mostly parallel to the compressive direction, are also observed at both P1 and P2. As the strain increased to the plastic deformation region (P3), these grains were reoriented to be perpendicular to the compressive direction. The maximum pole intensity of {0002} increases to 11.0 mrd at P4.

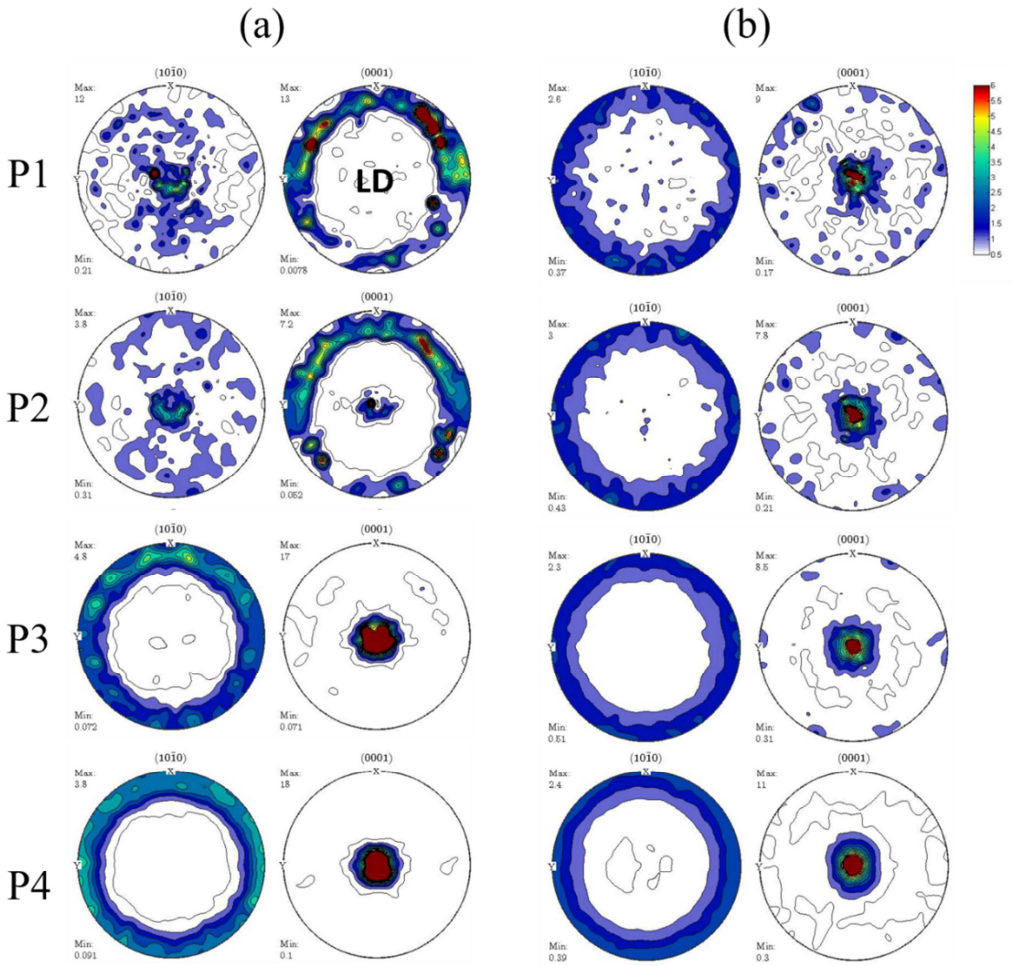

Fig. 4 {10$\bar{1}$0} and (0002) pole figures evolution from P1 to P4 for 0ED samples: (a) pure Mg; (b) Mg15Gd alloy. (The load direction is in the pole figure center.)

3.2.2 Compression with 45 ° to the extrusion direction (45ED)

Texture evolution for the 45ED samples during compressive deformation is shown in Fig. 5. The load direction is 45° to the basal planes for both pure Mg and the Mg15Gd alloy. At the early stage of compression (from P1 to P2), both pole figures show almost no change. Only the randomly distributed grains are rotated close to the maximum pole density location. With an increase in the strain, the basal planes of pure Mg were rotated perpendicular to the load

direction (from P2 to P4). On the other hand, the (0002) planes of the Mg15Gd alloy shifted in the same direction, i.e., the c-axes of the grains rotated ~30° away from the compressive direction.

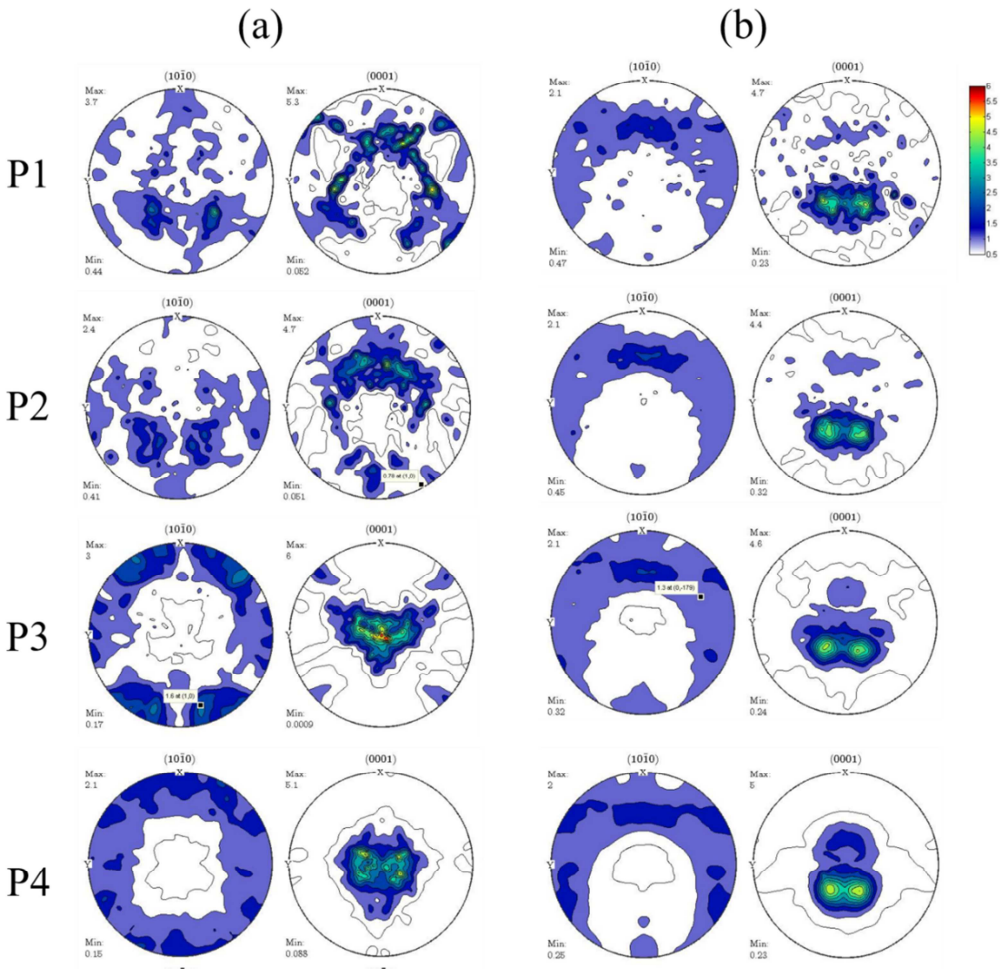

Fig. 5 {10$\bar{1}$0} and (0002) pole figure evolution from P1 to P4 for 45ED samples: (a) pure Mg; (b) Mg15Gd alloys. (The load direction is in the pole figure center.)

3.2.3 Compression with 90 ° to the extrusion direction (90ED)

Fig. 6 presents the {10$\bar{1}$0} and (0002) pole figure evolution during compression for the 90ED samples. Like other tests, both pole figures remain the same from P1 to P2. A significant difference in the texture evolution between these two materials is found at later stages. For

the pure Mg 90ED, like other pure Mg samples, the c-axes of the grains are parallel to the compressive direction after plastic deformation. However, in the early deformation of the Mg15Gd alloy, the development of four clusters at an angle interval of 60° is found in the (0002) pole figures after yielding (from P1 to P2). From P2 to P3, some (0002) grains have already rotated to the pole figure and are normal to the compressive direction after plastic deformation. After fracture (P4), most (0002) grains rotated with the basal planes normal to the compressive direction, and some are approximately 45° to the compressive direction.

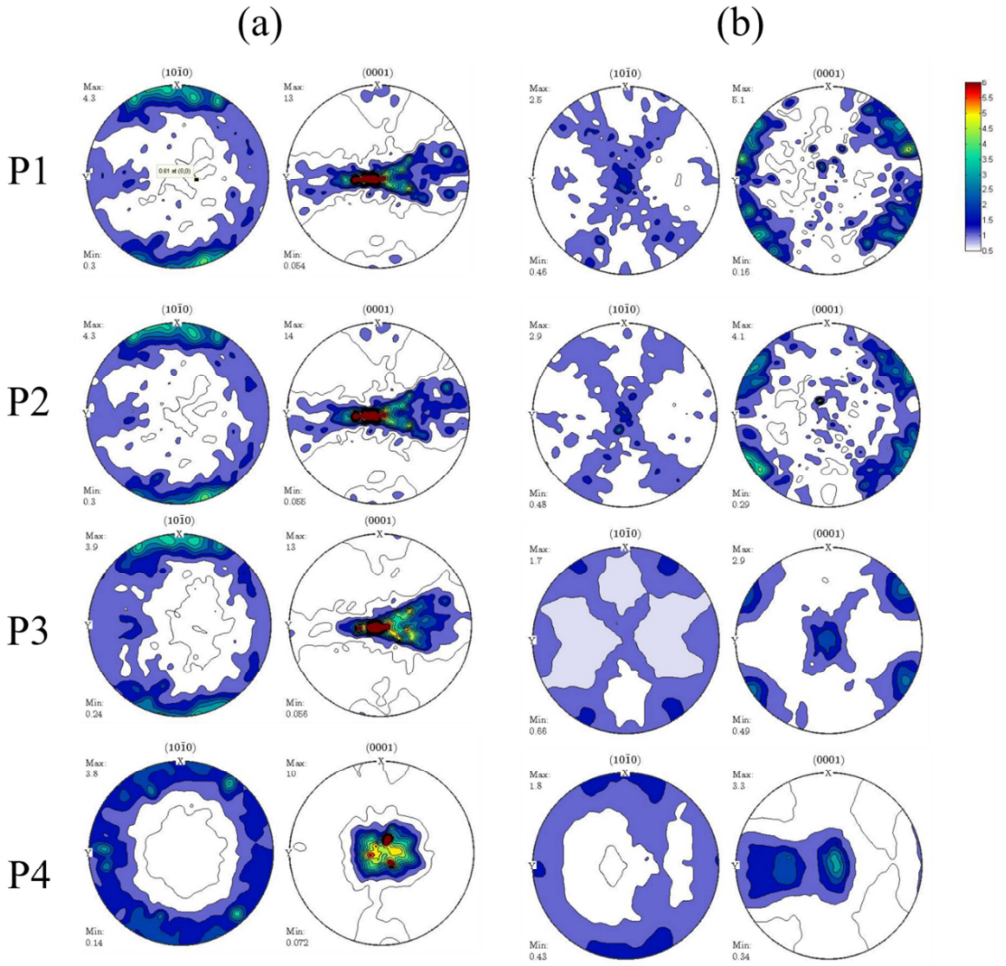

Fig. 6 {10$\bar{1}$0} and (0002) pole figures evolution of P1 to P4 for 90ED samples: (a) pure Mg; (b) Mg15Gd alloys. (The load direction is in the pole figure center.)

3.3 Lattice strain evolution during *in-situ* compression

3.3.1 Compression along extrusion direction (0ED)

Fig. 7 shows the integrated intensity evolution of the selected grain orientations for pure Mg and the Mg15Gd alloy, respectively. The grains have *c*-axes aligned in the transversal direction, as indicated by the texture of pure Mg. The intensity of (0002) in the transversal direction suddenly decreases at a stress of 33 MPa, which is contributed in part by grains undergoing twinning. Based on the texture results, it was found that a large number of grains are reoriented due to quasi-steady state plastic deformation, which leads to a great increase in the (0002) intensity in the axial direction. However, many grains have an orientation of the *c*-axis that follows the compression direction of the Mg15Gd alloy (Fig. 2(b)). The intensity data show a negligible difference during compression for the Mg15Gd alloy, indicating that there is little twinning in this alloy during deformation.

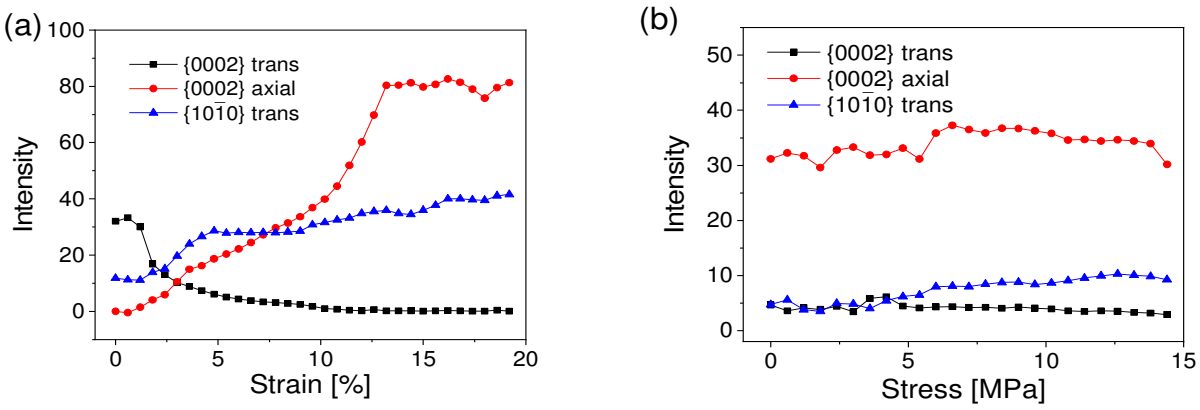

Fig. 7 Diffraction intensity of selected grain orientation for

(a) pure Mg and (b) Mg15Gd alloy of 0ED samples.

The lattice strain data for pure Mg and the Mg15Gd alloy are shown in Fig. 8. The black dotted horizontal lines represent the elastic response limit of the material, which is closely predicted by Young's modulus. Young's modulus results were measured with the impulse excitation technique using a resonant frequency and damping analyzer developed by IMCE, Belgium with a sample dimension of $6 \times 7 \times 45$ mm^3 [14]. For pure Mg and the Mg15Gd alloy, Young's modulus values are 44.1 and 44.5 GPa, respectively. Due to Passion's contraction, the elastic modulus in the transversal direction was predicted to be 1/3 of Young's modulus, serving as tensile strain. Macroscopic elastic behavior is indicated by the black dashed lines, which correspond closely to the elastic modulus, as shown in Fig. 8.

The pure Mg has a preference for the alignment of the *c*-axis perpendicular to the extrusion direction. As a consequence of the fiber texture, the lattice strains of the prismatic $\{10\bar{1}0\}$ planes of pure Mg follow these elastic predictions well before yield stress in the axial direction, and this outcome is closely predicted by Young's modulus (Fig. 7(a)). The $\{10\bar{1}2\}$ planes in the axial direction are under tensile stress before yielding, and a break occurs at the yield point. Little intensity of (0002) planes in the transversal direction is obtained after all grains are reoriented such that the *c*-axes are parallel to the load direction.

The majority of grains in Mg15Gd alloy have the *c*-axis parallel to the compression direction, and few grains show basal slip or twinning deformation modes in those grains. Consequently, the (0002) planes in the axial direction and $\{10\bar{1}0\}$ planes in the transversal direction show an increase in microstrain and follow the line of the slope of the elastic modulus (Fig. 8(b)). The

{10$\bar{1}$2} grains show the development of compressive strain in the transversal direction after yielding, which is an indication of basal slip or prismatic slip.

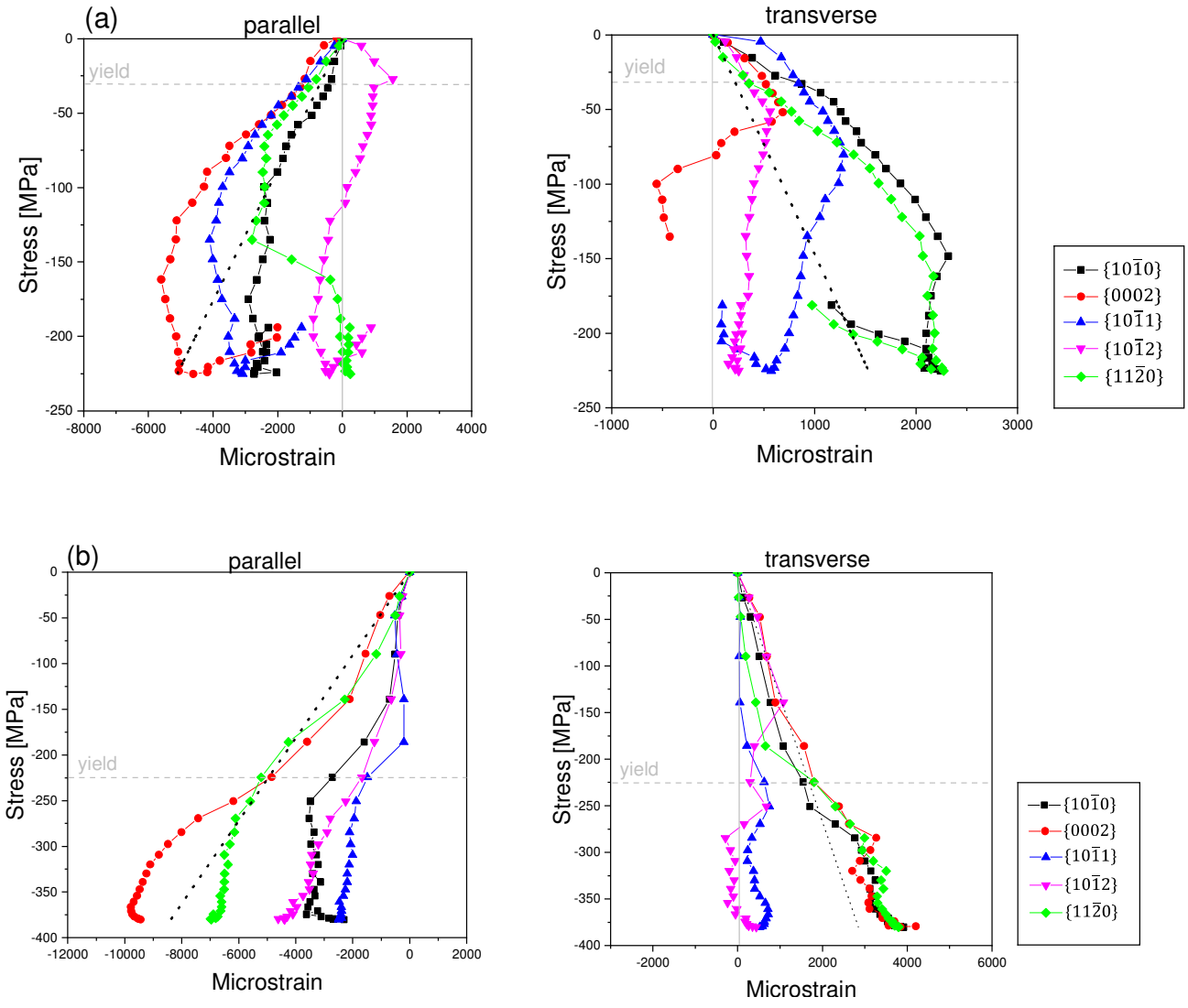

Fig. 8 Lattice strain response for 0ED test, (a) pure Mg and (b) Mg15Gd alloy.

3.3.2 Compression with 45 ° to extrusion direction (45ED)

The intensity evolution measured during the *in situ* testing of the 45ED samples is shown in Fig. 9. Both the studied materials have a similar intensity curve of (0002) grain planes in the transversal direction and {10$\bar{1}$1} planes in the axial direction. Most grains in the 45ED

samples have an orientation of 45° between *c*-axes and the compression direction, showing that the samples have a high Schmid factor for the basal slip system. Those grains undergo basal slip easily. The 45ED samples have the lowest yield strength as well as ultimate strength (Fig. 2).

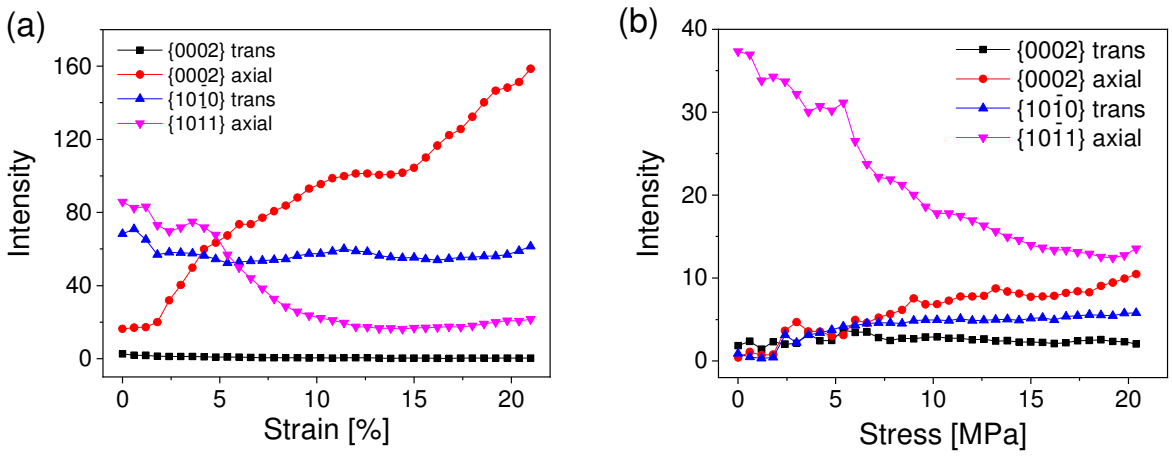

Fig. 9 Diffraction intensity evolution of selected grain orientations in the 45ED samples: (a) pure Mg and (b) Mg15Gd alloy.

The microstrain evolution for pure Mg and Mg15Gd are shown in Fig. 10(a) and (b), respectively. The data are significantly different between these two samples. The $\{10\bar{1}1\}$ grains of pure Mg parallel to the load direction show a linear increase in microstrain with increasing applied stress, consistent with elastic behavior, until 120 MPa. In the transversal direction, the $\{10\bar{1}0\}$ and $\{11\bar{2}0\}$ grains exhibit the development of tensile strain and follow the elastic curve. However, the (0002), $\{10\bar{1}1\}$ and $\{10\bar{1}2\}$ grains are compressive. For the Mg15Gd alloy, the microstrain of basal planes increases slightly before macroscopic yielding compared with the macrostrain, but after yielding, the microstrain greatly increased in the parallel direction. In the transversal direction, all the grains show tensile deformation before

macroscopic yielding. The group of $\{10\bar{1}2\}$ grains becomes compressive after macroscopic yielding.

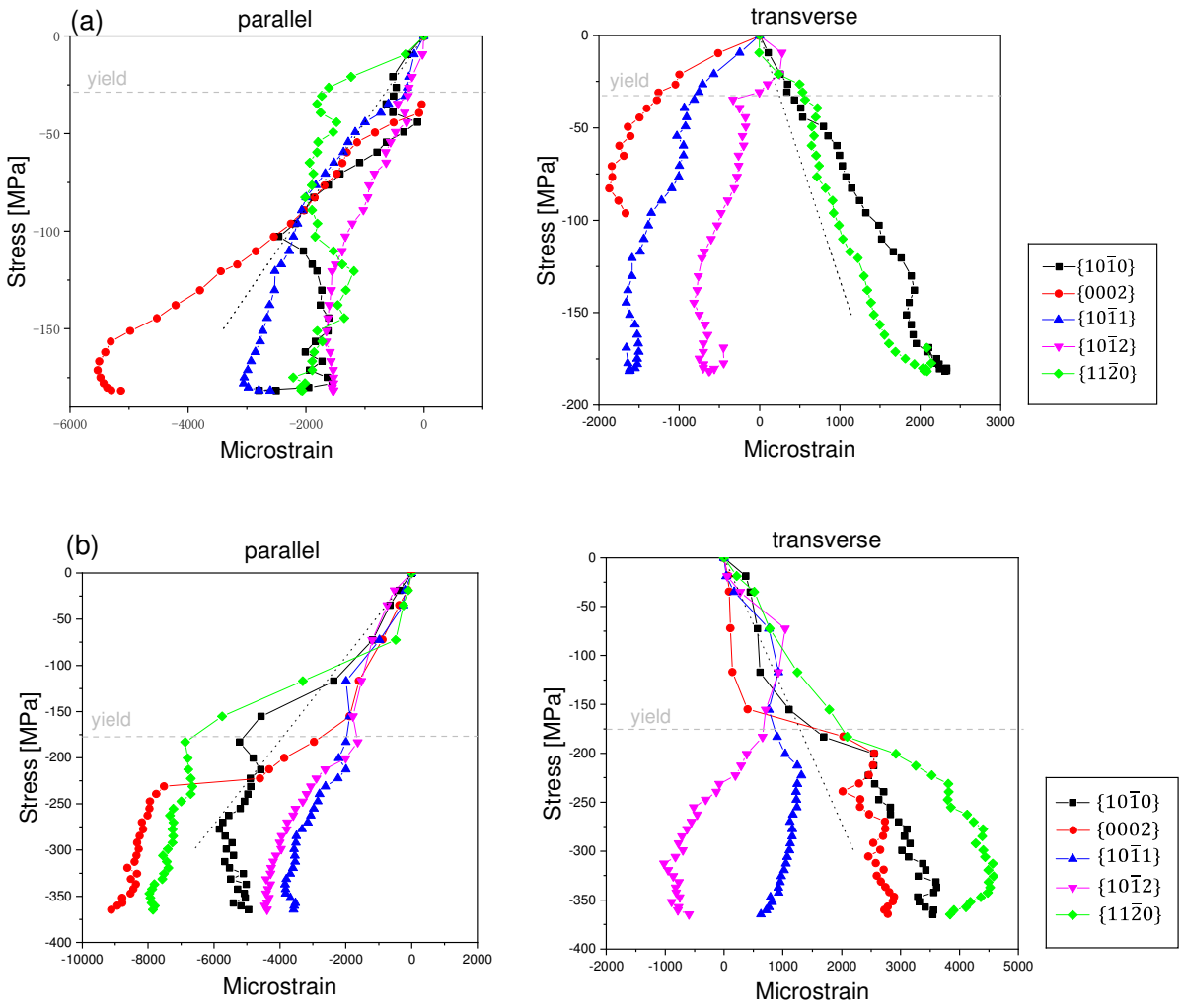

Fig. 10 Lattice strain evolution for 45ED test, (a) pure Mg and (b) Mg15Gd alloy.

3.3.3 Compression with 90 º to extrusion direction (90ED)

For pure Mg under 90ED compression tests, most grains laid on the (0002) planes perpendicular to the load direction, which have similar grain orientation with Mg15Gd ED specimen. However, the *in situ* measurement results of intensity variations for those two specimens are different. Due to prismatic slip is hard to be activated in pure Mg, the

intensities of (0002) and $\{10\bar{1}1\}$ planes in axial direction were changed after yielding (Fig. 11(a)). The flow curve of Mg15Gd shows the S-sharp which is related to $\{10\bar{1}2\}$ twinning. It is also demonstrated by intensity data (Fig. 11(b)). An obvious variation is observed in (0002) plane in compressive direction at yield point. The intensity of (0002) plane greatly increases from 0 to 10.0 mrd.

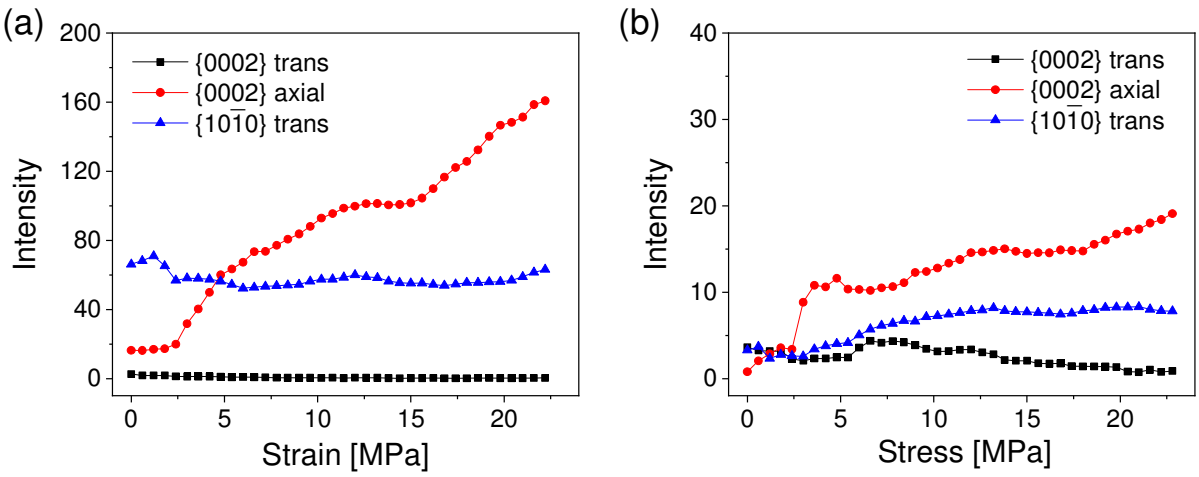

Fig. 11 Diffraction intensity evolution of selected grain orientation for the 90ED samples , (a) pure Mg and (b) Mg15Gd alloy.

Fig. 12 shows the internal microstrain data for the 90ED samples. It clearly shows three variations for the slope of pure Mg grains in the transversal direction, which are at the yield point, 60 MPa and 120 MPa, respectively (Fig. 11(a)). After yielding, except for the $\{11\bar{2}0\}$ planes, the planes in the transversal direction show the development of compressive strain rather than tensile strain. For Mg15Gd alloy, a change in the slope of the microstrain-stress curve is observed at 225 MPa, which is exactly the same as the change point in intensity data for the $\{10\bar{1}1\}$ prismatic planes in the axial direction.

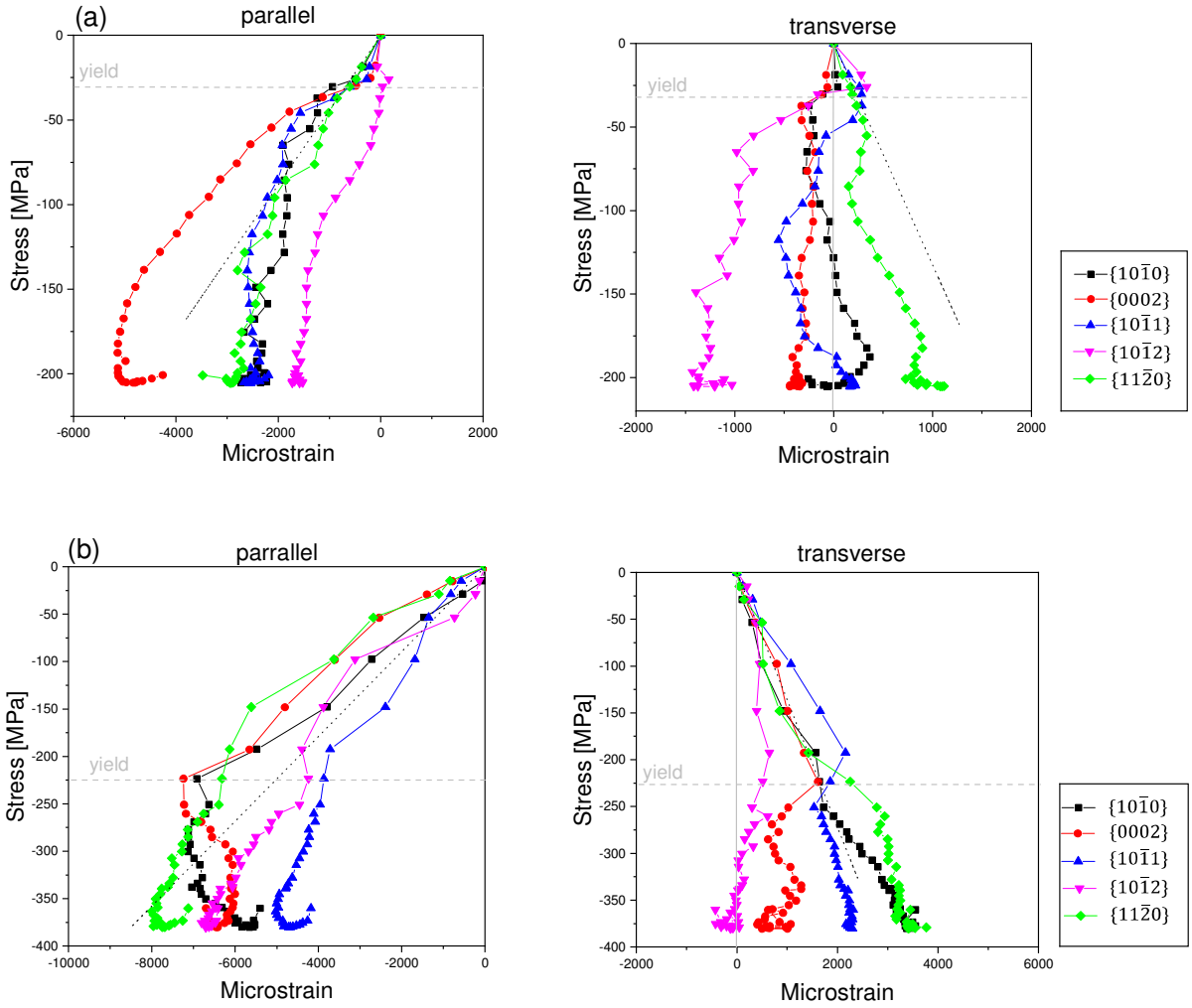

Fig. 12 Lattice strain evolution for the 90ED tests, (a) pure Mg and (b) Mg15Gd alloy.

4. Discussion

4.1 Effect of Gd on the texture evolution

After extrusion, the Mg15Gd alloy exhibits a specific texture wherein the basal planes (0002) are mainly oriented perpendicular to the ED. The authors explained that the lower c/a ration change the slip or twinning modes, which cause this kind of fiber texture [1]. This texture shows different texture evolution during compression compared with pure Mg. After yielding,

the (0002) planes of most grains of both the pure Mg and Mg15Gd alloy samples are perpendicular to the load axis at an angle of 0° to the ED. An interesting texture evolution has been found during compression for the Mg15Gd 45ED sample. The maximum pole intensity and its location undergo little change. In this case, the basal planes of both pure Mg and the Mg15Gd alloy are 45 degree from the load direction; the slip planes under compression should be (0002) basal planes. The grain of Mg15Gd alloy with a lower *c*/*a* ratio continually orientates though basal slip during deformation. However, the deformation of pure Mg is responsible for the activation of twinning. For the pure Mg 90ED sample, the texture shows little change at the early yield stage (from P2 to P3), and only a few grains with random distribution are in the vicinity perpendicular to the compressive direction. After the stress reached 200 MPa, a stable stress stage was found with an increase in the load (Fig. 2), and almost all grains rotated to the (0002) planes perpendicular to the compressive direction. On the other hand, the Mg15Gd alloy 90ED sample presents weaker texture during the compressive test. The pole intensity of (0002) near the compressive direction increases greatly in Fig. 6(b). The maximum pole intensity near the parallel to the compressive direction deceases after yielding.

4.2 Effect of Gd on the activation of slip and twinning

Sigmoidal hardening behavior is observed for all pure Mg samples (Fig. 2(a)). The “S-shape” appearance of the flow curve results from the orientation change associated with twinning, in which the twinned material is reoriented into a hard orientation. A number of investigations have pointed out that the yield stress and plastic deformation of the Mg alloy with a sharp

extruded texture under compressive load is controlled by the $<10\bar{1}0>\{10\bar{1}2\}$ extension twinning system [20]; this is also demonstrated by the case of the pure Mg 0ED sample. The diffraction intensity of the (0002) plane of the pure Mg 0ED sample in the transversal direction suddenly decreases to almost 0 after macroscopic yielding with 25 MPa stress. The intensity of the (0002) plane in the axial direction greatly increases at the yield point and steadily increases afterwards, which might be related to basal slip activity (Fig. 7 (a)). Hence, the break on the microstrain of $\{10\bar{1}2\}$ lattice planes in the axial direction also relies on the $<10\bar{1}0>\{10\bar{1}2\}$ twinning (Fig. 7(a)). However, this twinning system shows a lower activity in the Mg15Gd alloy 90ED sample, which has a similar grain orientation to the pure Mg 0ED. The addition of Gd decreases the c/a ratio to 1.617. The previous investigation shows that prismatic slip is easily activated with c/a < 1.621, so the diffraction intensity of the (0002) plane in the transversal direction remains stable even after yielding [21, 22]. The intensity slowly decreases through the macroscopic yielding to the plateau (350 MPa) and to 0. On the other hand, the intensity of the (0002) plane in the axial direction has saltation and increases at the yielding point (225 MPa). In this case, part of the grains are reoriented with the activation of $<10\bar{1}0>\{10\bar{1}2\}$ twinning.

The grains of pure Mg 45ED and Mg15Gd 45ED have similar orientations to the compressive direction. The angle between basal planes and the compressive direction is approximately 45 degrees. The microstrain-stress curves of both materials clearly indicate that the $\{10\bar{1}2\}$ grains have the highest microstrain before yielding. Basal slip controls the early deformation during compression. Based on the engineering stress-strain curves, it is confirmed that the Gd

in solid solute greatly strengthens the basal slip of pure Mg. Different deformation behaviors are observed in pure Mg and the Mg15Gd alloy when the grains rotate to hard orientations with an additional load. For pure Mg, in the transversal direction, only prismatic grains develop tensile strains, and even the basal grains are under compressive strains. Combined with the intensity curve of the (0002) plane in the axial direction, the contraction twinning system controls the newly formed grain deformation. On the other hand, it is most likely that <c+a> slip controls the subsequent deformation for the Mg15Gd 45ED, which leads to a stable location of maximum pole intensity in texture analysis.

The pure Mg 90ED and Mg15Gd 0ED samples have similar orientations, in which most of the grains have their *c*-axes in the loading direction. The intensity data indicate that these two samples have significantly different deformation mechanisms. The deformation is obviously controlled by contraction twinning for pure Mg, but there is negligible twinning in the Mg15Gd alloy. For pure Mg, the majority of grains under 90ED compression are poorly oriented for basal slip or $\{10\bar{1}2\}$ extension twinning. As seen in the microstrain data, the internal strain of the $\{10\bar{1}2\}$ and $\{10\bar{1}1\}$ planes in the transversal direction changes from tension to compression. Consequently, these grains are moved by $\{10\bar{1}1\}$ contraction twining, and the twinned grains have an approximately 57 degree rotation. Due to the lower *c*/*a* ratio, prismatic slip is activated in Mg15Gd 0ED. Therefore, the internal strains of the $\{10\bar{1}2\}$ and $\{10\bar{1}1\}$ planes in both directions have very small values.

5. Conclusion

The texture evolution and lattice strain of extruded pure Mg and the Mg15Gd alloy have been studied with *in situ* synchrotron radiation diffraction in three different compression directions. The following conclusions were drawn:

- A strong fiber texture corresponding to the basal planes {0002} perpendicular to the ED is formed in the Mg alloy with a high Gd solid solute content.
- Prismatic slip has been activated in Mg15Gd due to the decreased *c*/*a* ratio resulting from the addition of Gd under compression. During compressive deformation of 0ED Mg15Gd, the macro yield occurs at 225 MPa, which is dominated by prismatic slip.
- The $\{10\bar{1}2\}$ extension twinning is a major deformation mode during compression for pure Mg. Twinning occurs at the yielding point in the 0ED and 90ED pure Mg samples, and the yield stresses are approximately 25 MPa. For 45ED pure Mg samples, basal slip also plays an important role during its early deformation stage.
- The $\{10\bar{1}1\}$ contraction twinning controls the newly formed grains, and increasing deformation at the plateau stage is present in 45ED and 90ED pure Mg.

Acknowledgement

This The authors would like to acknowledge the help of Mr. Günther Meister (MagIC, HZG) during casting. The authors thank Prof. Walter Reimers (FMW, TU Berlin) for offering help of extrusion processing. The authors gratefully thank Dr. Heinz-Guenter Brokmeier and Bernd Schwebke (GEMS, HZG) for their help during synchrotron radiation test and Dr.

Longlong Hao (Chongqing University) for his help during HAADF-STEM test. The authors thank Dr. Jan Bohlen (MagIC, HZG) and A/Prof. Bo Song (Southwest University) for their fruitful discussion. The present work was co-supported by the National Key Research and Development Program of China (No. 2016YFB0301100).

References

[1] T.B. Britton, F.P.E. Dunne, A.J. Wilkinson, On the mechanistic basis of deformation at the microscale in hexagonal close-packed metals, Proceedings of the Royal Society A: Mathematical, Physical and Engineering Science 471(2178) (2015) 20140881. http://dx.doi.org/10.1098/rspa.2014.0881

[2] A.L. Oppedal, H.E. Kadiri, C.N. Tomé, J.C. Baird, S.C. Vogel, M.F. Horstemeyer, Limitation of current hardening models in predicting anisotropy by twinning in hcp metals: Application to a rod-textured AM30 magnesium alloy, Magnesium Technology 2011. https://doi.org/10.1007/978-3-319-48223-1_59

[3] H. Yoshinaga, R. Horiuchi, Deformation mechanisms in magnesium single crystals compressed in the direction parallel to hexagonal axis, Trans. Japan Inst. Met. 4 (1963) 1-8.

[4] H. Conrad, W.D. Robertson, Effect of temperature on the flow stress and strain-hardening coefficient of magnesium single crystals, JOM 9 (1957) 503-512.

[5] N. Stanford, R. Cottam, B. Davis, J. Robson, Evaluating the effect of yttrium as a solute strengthener in magnesium using in situ neutron diffraction, Acta Materialia 78 (2014) 1-13. https://doi.org/10.1016/j.actamat.2014.06.023

[6] S.R. Agnew, R.P. Mulay, F.J. Polesak, C.A. Calhoun, J.J. Bhattacharyya, B. Clausen, In situ neutron diffraction and polycrystal plasticity modeling of a Mg–Y–Nd–Zr alloy: Effects of precipitation on individual deformation mechanisms, Acta Materialia 61 (2013) 3769-3780. https://doi.org/10.1016/j.actamat.2013.03.010

[7] S.R. Agnew, C.N. Tomé, D.W. Brown, T.M. Holden, S.C. Vogel, Study of slip mechanisms in a magnesium alloy by neutron diffraction and modeling, Scripta Materialia 48(8) (2003) 1003-1008. https://doi.org/10.1016/S1359-6462(02)00591-2

[8] E.D. Levine, Deformation mechanisms in titanium at low temperatures, Trans. Metall. Soc. AIME 236 (1966) 1558.

[9] E.J. Rapperport, Room temperature deformation processes in zirconium, Acta Metallurgica 7 (1959) 254-260.

[10] J. Bohlen, S. Yi, D. Letzig, K.U. Kainer, Effect of rare earth elements on the microstructure and texture development in magnesium–manganese alloys during extrusion,

Materials Science and Engineering: A 527(26) (2010) 7092-7098. https://doi.org/10.1016/j.msea.2010.07.081

[11] N. Stanford, M.R. Barnett, The origin of “rare earth” texture development in extruded Mg-based alloys and its effect on tensile ductility, Materials Science and Engineering: A 496(1-2) (2008) 399-408. https://doi.org/10.1016/j.msea.2008.05.045

[12] K. Hantzsche, J. Bohlen, J. Wendt, K. Kainer, S. Yi, D. Letzig, Effect of rare earth additions on microstructure and texture development of magnesium alloy sheets, Scripta Materialia 63(7) (2010) 725-730. https://doi.org/10.1016/j.scriptamat.2009.12.033

[13] H. Okamoto, Gd-Mg (Gadolinium-Magnesium), Journal of phase equilibria 14(4) (1993) 534-535.

[14] Y. Xu, L. Wang, M. Huang, F. Gensch, K.U. Kainer, N. Hort, The Effect of Solid Solute and Precipitate Phase on Young’s Modulus of Binary Mg–RE Alloys, Advanced Engineering Materials (2018). https://doi.org/10.1002/adem.201800271

[15] G. Nolze, R. Hielscher, Orientations – perfectly colored, Journal of Applied Crystallography 49(5) (2016) 1786-1802. https://doi.org/10.1107/S1600576716012942

[16] A.P. Hammersley, S.O. Svensson, M. Hanfland, A.N. Fitch, D. Hausermann, Two-dimensional detector software: From real detector to idealised image or two-theta scan, High Pressure Research 14(4-6) (1996) 235-248.

[17] S. Biswas, S. Suwas, R. Sikand, A.K. Gupta, Analysis of texture evolution in pure magnesium and the magnesium alloy AM30 during rod and tube extrusion, Materials Science and Engineering: A 528(10-11) (2011) 3722-3729. https://doi.org/10.1016/j.msea.2011.01.021

[18] H. Zengin, Y. Turen, Effect of La content and extrusion temperature on microstructure, texture and mechanical properties of Mg-Zn-Zr magnesium alloy, Materials Chemistry and Physics 214 (2018) 421-430. https://doi.org/10.1016/j.matchemphys.2018.04.110

[19] R.A. Young, The Rietveld Method, Oxford University Press, New York, USA, 1993.

[20] O. Muránsky, M.R. Barnett, V. Luzin, S. Vogel, On the correlation between deformation twinning and Lüders-like deformation in an extruded Mg alloy: In situ neutron diffraction and EPSC.4 modelling, Materials Science and Engineering: A 527(6) (2010) 1383-1394. https://doi.org/10.1016/j.msea.2009.10.018

[21] M. Yoo, S. Agnew, J. Morris, K. Ho, Non-basal slip systems in HCP metals and alloys: source mechanisms, Materials Science and Engineering: A 319 (2001) 87-92. https://doi.org/10.1016/S0921-5093(01)01027-9